PCCP

RSC Publishing

PAPER

View Article Online
View Journal | View Issue

Published on 12 September 2013. Downloaded by Michigan State University on 20/01/2016 02:50:59.

Cite this: *Phys. Chem. Chem. Phys.*, 2013, **15**, 17537

The visible transmittance and solar modulation ability of VO_2 flexible foils simultaneously improved by Ti doping: an optimization and first principle study†

Shi Chen,[a] Lei Dai,[a] Jianjun Liu,[a] Yanfeng Gao,*[ab] Xinling Liu,[a] Zhang Chen,[a] Jiadong Zhou,[a] Chuanxiang Cao,[a] Penggang Han,[a] Hongjie Luo[ab] and Minoru Kanahira[a]

Received 15th May 2013,
Accepted 19th July 2013

DOI: 10.1039/c3cp52009a

www.rsc.org/pccp

The Mott phase transition compound vanadium dioxide (VO_2) shows promise as a thermochromic smart material for the improvement of energy efficiency and comfort in a number of applications. However, the use of VO_2 has been restricted by its low visible transmittance (T_{vis}) and limited solar modulation ability (ΔT_{sol}). Many efforts have been made to improve both of these limitations, but progress towards the optimization of one aspect has always come at the expense of the other. This paper reports that Ti doping results in the improvement of both the T_{vis} and ΔT_{sol} of VO_2-nanoparticle-derived flexible foils to the best levels yet reported. Compared with an undoped VO_2 foil, a 15% increase (from 46.1% to 53%) in T_{vis} and a 28% increase (from 13.4% to 17.2%) in ΔT_{sol} are achieved at a Ti doping level of 1.1%, representing the best performance reported for similar foils or films prepared using various methods. Only a defined doping level of less than 3% is beneficial for simultaneous improvement in T_{vis} and ΔT_{sol}. First principle calculations suggest that an increase in the intrinsic band gap of VO_2 (M) and the reduced electron density at Fermi level of VO_2 (R) cooperate to result in the improvement of ΔT_{sol} and that an enhancement in the optical band gap of VO_2 (M) leads to the increase of T_{vis}.

Introduction

The Mott-phase transition material vanadium dioxide (VO_2) is a key material in thermochromic smart window applications as it exhibits a reversible transformation from an infrared-transparent semiconductive state at low temperatures to an infrared-reflective metallic state at high temperatures while maintaining visible transmittance.[1–6] Due to these properties, VO_2 is the most promising material for smart windows compared with other inorganic and polymer based thermochromic materials.[7,8] However, low visible transmittance (T_{vis}, integral transmittance between 380 nm and 780 nm) and insufficient solar modulation ability (ΔT_{sol}, $\Delta T_{sol} = T_{sol,25^\circ C} - T_{sol,90^\circ C}$, T_{sol}, integral transmittance between 240 nm and 2600 nm) limit the performance of VO_2 in smart windows.

To meet the requirements for practical thermochromic fenestration, VO_2 materials must satisfy the following criteria: $T_{vis} > 40\%$ and $\Delta T_{sol} > 10\%$.[9] The current strategies employed in hopes of improving these values primarily involve the syntheses of nanoporous films,[10] construction of composite films,[11,12] deposition of antireflective layers[13–15] and doping.[16,17] Our previous research suggests that ΔT_{sol} may be increased from 7.0% to 14.1% with a slight decrease in T_{vis}, from 45.3% to 43.3%, by optimizing the porosity of the VO_2 film. The inclusion of nanopores in VO_2 films serves to decrease the refractive index and the extinction coefficient, which, in conjunction with the optimization of the material thicknesses, results in the depression of reflection in both the visible and infrared regions.[10] Optical calculations performed by Granqvist *et al.* indicate that VO_2 nanoparticles distributed in a dielectric matrix have relatively higher T_{vis} and ΔT_{sol} than pure VO_2 films,[11] which we have experimentally confirmed through the synthesis of a VO_2–ZrV_2O_7 composite film of significantly enhanced T_{vis} (from 32.3% at Zr–V = 0 to 53.4% at Zr–V = 0.12).[12] The addition of antireflective layers could improve both T_{vis} and ΔT_{sol}. One example of this improvement is a five-layered film (TiO_2–VO_2–TiO_2–VO_2–TiO_2) possessing a much higher T_{vis} = 45% and ΔT_{sol} = 12.1% than found in single-layered VO_2 films (T_{vis} = 41% and ΔT_{sol} = 6.7%).[15] A TiO_2–VO_2 double-layered film prepared through the deposition

[a] *State Key Laboratory of High Performance Ceramics and Superfine Microstructure, Shanghai Institute of Ceramics, Chinese Academy of Sciences, 1295 Dingxi, Shanghai 200050, China. E-mail: yfgao@shu.edu.cn; Fax: +86-21-6990-6218; Tel: +86-21-6990-6218*

[b] *School of Materials Science and Engineering, Shanghai University, 99 Shangda, Shanghai 200444, China*

† Electronic supplementary information (ESI) available. See DOI: 10.1039/c3cp52009a

Published on 12 September 2013. Downloaded by Michigan State University on 20/01/2016 02:50:59.

of an antireflective layer on a nanoporous VO_2 film exhibited a relatively higher T_{vis} (49.5%) and ΔT_{sol} (15.1%).[13] In general, nanoporous morphologies and formation of composites with highly transparent matrices usually enhance either T_{vis} or ΔT_{sol} but not both, while optimized antireflective layers can simultaneously increase both of these crucial parameters. However, antireflective layers inevitably increase material consumption and processing complexity, making accurate control over the refractive index and thickness particularly problematic. The challenge of simultaneously improving T_{vis} and ΔT_{sol} to levels required for their practical application is daunting.

Doping is a strategy that is normally employed to lower the phase transition temperatures for bulk VO_2 from 68 °C to near room temperature (−23 °C/at.% W,[18] −20 °C/at.% F[17] and −15 °C/at.% Mo[19]) and to modify hysteresis loop widths (Ti,[20] Nb[21]). Some doping systems also produce improvements in T_{vis}.[16,17,22–24] A recent report on a foil derived from Mg-doped VO_2-nanoparticles shows a blue-shift in the absorption edge from 490 nm (2.53 eV) to 440 nm (2.82 eV) at a Mg doping level of 3.8%, resulting in an increase in T_{vis} (from 45.3% to 54.2%).[23] This observation is in agreement with a previous finding that Mg doping at 7.2% can widen the optical band gap of VO_2 from 1.67 eV to 1.95 eV, significantly decreasing luminous absorption and leading to a substantial improvement in T_{vis} (from 39% to 51%).[16,24] Doping with F at 2.0% causes a blue-shift in the absorption edge of VO_2 from 445 nm (2.79 eV) to 415 nm (2.99 eV), resulting in an increased T_{vis} and a film of visibly lighter color.[17] However, Mg or F doping only enhances T_{vis}; simultaneous increases in T_{vis} and ΔT_{sol} are still a challenge.

Among doping elements, Ti^{4+} possesses a similar electronic structure and ionic radius to V^{4+} and has attracted considerable attention as a dopant for modifying the thermochromic properties of VO_2.[20,21,25–28] Most studies have focused on the ability of Ti^{4+} to improve the temperature coefficients of resistance (TCR, 3.00%/°C,[20] 5.12%/°C[28] and 24.8%/°C[21]) and to decrease hysteresis loop widths (ΔT, declining from 38.2 °C to 3.5 °C[27] or from 6 °C to 1 °C[21]). Doping with Ti also allows for complete control of the dielectric constants,[25] T_{vis} and ΔT_{sol}[26,27] of a VO_2 film. Hu *et al.* reported increasing T_{vis} and decreasing ΔT_{sol} values with increasing Ti concentrations in a Ti-doped VO_2 film, however, the minimum doping level was 28.6%.[26] Our previous work showed almost no change in the near infrared switching efficiency (ΔT_{2000}, $\Delta T_{2000} = T_{2000,25°C} - T_{2000,90°C}$, T_{2000}, transmittance at a fixed wavelength of 2000 nm) at a Ti doping level below 7.4% and significant decreases in ΔT_{2000} above 7.4% doping.[27] No study to date has examined the effect of Ti doping on T_{vis} and ΔT_{sol} at doping levels below 5%, and no attempt has been made towards the simultaneous enhancement of T_{vis} and ΔT_{sol}. Moreover, the aforementioned studies are based on Ti-doped VO_2 films; no investigation of Ti-doped VO_2 nanoparticles have been performed, despite the fact that the formation of VO_2 flexible foils based on VO_2 nanoparticles is a cost-effective alternative synthesis technique for VO_2 smart windows.[23,29,30]

With these considerations in mind, we investigated Ti-doped VO_2 nanoparticles at low doping levels and monitored the effects of doping on nanoparticle-derived VO_2 polymer composites foils. Compared with an undoped VO_2 foil, 15% (from 46.1% to 53%) and 28% (from 13.4% to 17.2%) increases in T_{vis} and ΔT_{sol}, respectively, are achieved at 1.1% Ti doping, representing the most promising values of T_{vis} and ΔT_{sol} in VO_2 foils or films prepared using available methods. The results also suggest that only a defined doping level of less than 3% is effective in the simultaneous improvement of T_{vis} and ΔT_{sol}. To explain this phenomenon, the crystalline structures, element valence states and phase transitions of Ti-doped VO_2 nanoparticles were analyzed experimentally and a first-principles calculation was performed to theoretically explain the effects of Ti doping on the optical properties.

Experimental and theoretical methods

Preparation of Ti-doped VO_2 nanoparticles and VO_2–PU composite foils

All reagents were of analytical grade and were used without further purification. In a typical hydrothermal synthesis, 0.125 g V_2O_5 powder and the requisite quantity of $TiCl_4$ dopant were added into 40 mL of 0.15 M aqueous $H_2C_2O_4{\cdot}2H_2O$ to form a yellowish slurry. The slurry was stirred for 10 min and transferred to a 50 mL Teflon-lined stainless-steel autoclave. The autoclave was maintained at 240 °C for 24 h and then air-cooled to room temperature. The final product was collected *via* centrifugation, washed three times with deionized water and dried in a vacuum oven at 50 °C for 12 h. The VO_2–polyurethane (PU) thermochromic composite foils were prepared according to the following step.[23,29,30] The as-prepared Ti-doped VO_2 nanoparticles were dispersed in deionised water with continuous stirring for 10 min and an appropriate quantity of the silane coupling agent KH-570 was added with ultrasonic treatment for approximately 30 min. Then, PU was added gradually with stirring over 10 min. Finally, the suspension was uniformly cast onto a polyethylene terephthalate (PET) substrate using an automatic coating machine and dried at 80 °C for 1 min. The VO_2–PU composite foils exhibited excellent flexibility in Fig. S1 (ESI†).

Characterization

The morphologies and element distributions of the resulting powders were analysed *via* transmission electron microscopy (TEM, JEM2010, JEOL, Japan) with an energy-dispersive spectrometer (EDS) attachment. The crystalline structures of the resultant products were characterized with a Rigaku D/max 2550 V X-ray diffractometer (Japan) with Cu Kα radiation (λ = 0.15406 nm). The final doping ratios were confirmed by inductively coupled plasma measurements (ICP, Thermoelectric Corporation, IRIS Intrepid). X-ray photoelectron spectrometry (XPS) was performed with an Axis ultra DLD instrument using monochromatic Al Kα radiation after 1 keV argon-ion etching for 10 s. The phase transition temperatures of the products were measured *via* differential scanning calorimetry (DSC, DSC200F3, NETZSCH) in nitrogen flow in the temperature range from 0 °C to 100 °C at a heating rate of 10 °C min^{-1}. The spectrum characteristics of the VO_2–PU composite foils were monitored in the range of 240–2600 nm on a Hitachi U-4100 UV visible-near-IR

 This journal is © the Owner Societies 2013

Published on 12 September 2013. Downloaded by Michigan State University on 20/01/2016 02:50:59.

spectrophotometer equipped with a film heating unit. For all samples, the integral visible transmittance (T_{vis}, 380–780 nm), near infrared transmittance (T_{ni}, 750–1500 nm) and solar transmittance (T_{sol}, 240–2600 nm) were obtained based on the measured spectra using the following equation:

$$T_i = \int \varphi_i(\lambda) T(\lambda) d\lambda / \int \varphi_i(\lambda) d\lambda \quad (1)$$

$$\Delta T_{sol} = T_{sol}(T < T_c) - T_{sol}(T > T_c) \quad (2)$$

$$\Delta T_{ni} = T_{ni}(T < T_c) - T_{ni}(T > T_c) \quad (3)$$

where $T(\lambda)$ denotes the transmittance at wavelength λ, i denotes 'vis', 'ni' or 'sol' for the calculations, T and ΔT_{sol} are the temperature and solar modulation ability, φ_{vis} is the standard luminous efficiency function for photopic vision, and φ_{sol} and φ_{ni} are the solar irradiance spectra for the air mass 1.5 (corresponding to the sun standing 37° above the horizon).

Ab initio calculations

Periodic DFT calculations were performed using the VASP code.[31,32] The exchange and correlation items were described using a generalized gradient approximation (PBE-GGA).[33,34] To improve the treatment of electronic correlations in our DFT calculations, the Hubbard on-site repulsion U was taken into account within the so-called GGA + U approximation.[35] The effective strength of the interaction (U_{eff}, $U_{eff} = U - J$) was set at 4.6 eV, in which U (5.3 eV) is the on-site Hubbard repulsion and J (0.7 eV) is Hund's exchange interaction.[36,37] The electron–ion interactions were described using the projector augmented wave (PAW) method, and valence electrons were treated explicitly with a plane-wave basis set at a cut-off energy of 400 eV.

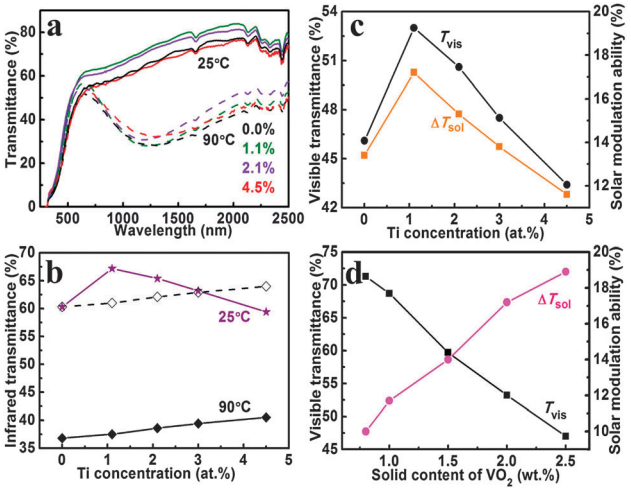

Fig. 1 The optical properties of a pure VO_2 and Ti-doped VO_2 foils with various Ti doping levels. (a) The transmittance spectra at 25 °C and 90 °C. (b) The near-infrared transmittance of the foils. The dotted line is the translated line of near-infrared transmittance at 90 °C. (c) The visible transmittance and solar modulation ability. (d) The visible transmittance and solar modulation ability of the 1.1% Ti-doped VO_2 foil with different solid contents of VO_2.

Table 1 Current and previously reported results of the visible transmittance and solar modulation ability of VO_2 films or foils

System	T_{vis} (%)	ΔT_{sol} (%)
Singer-layered VO_2 film[14]	41	6.7
TiO_2–VO_2–TiO_2–VO_2–TiO_2 five-layered film[15]	39	13.0
TiO_2–VO_2 double-layered film[13]	49	15.1
Mg-doped VO_2 film[16]	51	4.0
SiO_2–VO_2 core–shell composite foil[29]	29	13.6
VO_2–ATO–polymer composite foil[30]	53	11.7
1.1% Ti doped VO_2 foil (this work)	53	17.2

Results and discussion

Solar energy between 250 nm and 1500 nm accounts for nearly 90% of the total energy in the solar irradiance spectra.[38,39] This fact suggests that transmittance differences across the Mott phase transition in this wavelength region dominate the solar modulation ability of VO_2 foils. Before and after the phase transition, the VO_2 foils exhibited distinct transmittance differences in the near infrared region between 750 nm and 1500 nm, while their visible transmittance between 250 nm and 750 nm remained unchanged (Fig. 1a). Thus, the integral transmittance difference in the near infrared region ($\Delta T_{ni} = T_{ni,25°C} - T_{ni,90°C}$; T_{ni}, integral transmittance between 750 nm and 1500 nm) dominates the ΔT_{sol} of VO_2 foils. As shown in Fig. 1b, compared to an undoped VO_2 foil, T_{ni} at both 25 °C and at 90 °C increased at Ti doping levels below 3%, with a larger increase 25 °C than at 90 °C, resulting in an increase of ΔT_{ni} and an enhanced ΔT_{sol} (Fig. 1c). From Fig. 1c, the maximum values for T_{vis} and ΔT_{sol} were obtained with 1.1% Ti doping, exhibiting a 15% increase (from 46.1% to 53%) in T_{vis} and a 28% increase (from 13.4% to 17.2%) in ΔT_{sol} compared to an undoped VO_2 foil. Amazingly, Ti doping at defined levels can simultaneously enhance the T_{vis} and ΔT_{sol} of VO_2 foils, achieving the best values (T_{vis} = 53.0%, ΔT_{sol} = 17.2%) measured for VO_2 foils or films prepared using available methods (Table 1). When the Ti content was increased to 3.0%, the foil showed a slightly higher T_{vis} (47.5%) and ΔT_{sol} (13.8%) than the T_{vis} (46.1%) and ΔT_{sol} (13.4%) for an undoped VO_2 foil. The T_{vis} and ΔT_{sol} further declined to 43.4% and 11.6%, respectively, at 4.5% Ti. This trend indicated that low-level Ti doping below 3% was beneficial for simultaneous improvement of T_{vis} and ΔT_{sol}.

The response of T_{vis} and ΔT_{sol} of the 1.1% Ti-doped VO_2 foil to the variation in the solid content of VO_2 nanoparticles (Fig. 1d) suggested that several mixtures could meet the requirement of $T_{vis} > 40\%$ and $\Delta T_{sol} > 10\%$. T_{vis} reached a maximum value of 71.3% with ΔT_{sol} at 10%; while the ΔT_{sol} maximum of 18.9% was achieved as T_{vis} was still 47%, suggesting a good balance between T_{vis} and ΔT_{sol}. A comparison of the T_{vis} and ΔT_{sol} of VO_2 films prepared using different methods (Fig. 2) clearly shows that our results are the closest to theoretical values. The experimental T_{vis} and ΔT_{sol} values of the 1.1% Ti doped VO_2 foil constructed with VO_2 nanoparticles were superior to those of single-layered films,[40] porous films[41] and multi-layered films,[13,14] and they approached the calculated values for composite films.[11]

To understand the effects of Ti doping on the optical properties of the Ti-doped VO_2 composite foils, the crystalline

Published on 12 September 2013. Downloaded by Michigan State University on 20/01/2016 02:50:59.

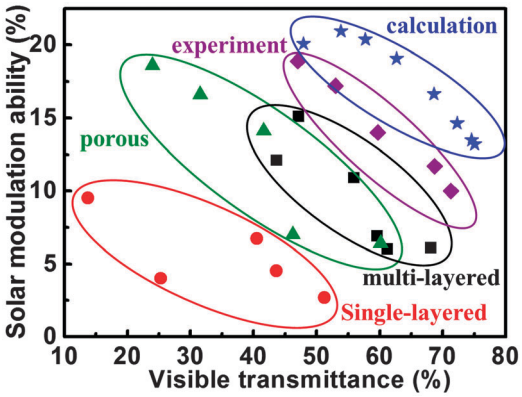

Fig. 2 Visible transmittance and solar modulation ability of VO_2 films prepared using different methods. Calculated results were obtained with effective medium theory.[11] Experimental results were obtained from this study. The results for single-layered films, porous films, multi-layered films and calculation were reprinted with permission (Y. Gao, H. Luo, Z. Zhang, L. Kang, Z. Chen, J. Du and M. Kanehira, *Nano Energy*, 2012, **1**, 221–226). Copyright (2012) Elsevier.

structures, element valence states and phase transitions were analyzed experimentally and theoretically *via* first principles calculations.

All XRD peaks for the $Ti_xV_{1-x}O_2$ powders could be indexed to VO_2 (M1) phase and no other phases were detected (Fig. 3a). Because the radius of Ti^{4+} (60.5 pm) is close to that of V^{4+} (58 pm), no significant migration in the diffraction peaks was observed at Ti doping levels below 4.5%. No obvious broadening of the diffraction peaks was observed, suggesting that the grain size was nearly unchanged. The lattice parameters in Table 2 were calculated from interplanar distances using the following equation:

$$\frac{1}{d^2} = \frac{h^2}{a^2 \sin^2\beta} + \frac{k^2}{b^2} + \frac{l^2}{c^2 \sin^2\beta} - \frac{2lh\cos\beta}{ca\sin^2\beta} \quad (4)$$

At a doping level of 4.5%, the lattice parameters for *a* and *c* increased from 5.742 to 5.768 Å and from 5.344 to 5.371 Å, respectively; meanwhile, that for *b* decreased from 4.528 to 4.510 Å, representing a ~0.7% expansion in the overall volume. The 1.1%, 2.1% and 3.0% Ti doped samples experienced volume expansions of 0.02%, 0.06% and 0.3%, respectively (Fig. 3b). A smaller lattice distortion was observed at Ti doping levels below 2.1% than 4.5%, which was likely beneficial for the thermochromic performance of the VO_2 nanoparticles.

For 1.1% Ti-doped VO_2, the binding energy of the V $2p_{3/2}$ peaks, centered at 516.0 eV (Fig. 3c), was in good agreement with the 515.8 eV value of pure VO_2.[42] The difference in the binding energies between O1s and V $2p_{3/2}$ was 14.5 eV, consistent with the literature value of 14.2 eV.[41] The binding energies of Ti $2p_{3/2}$ and Ti $2p_{1/2}$ were observed at approximately 459 eV and 464.9 eV (Fig. 3d), showing good agreement with the difference in these binding energies previously reported for Ti^{4+} in particles (5.7 eV),[43] implying that the carrier concentration experienced no significant change in the system. Moreover, the electronegativity of Ti (1.63) was close to that of V (1.54), indicating no distinct charge transfer from Ti^{4+} ions weakening the V–V pairs, in contrast to materials doped with W^{6+} or Mg^{2+}.[16,44] These results indicated that Ti^{4+} doping maintained the electronic structure stability of VO_2.

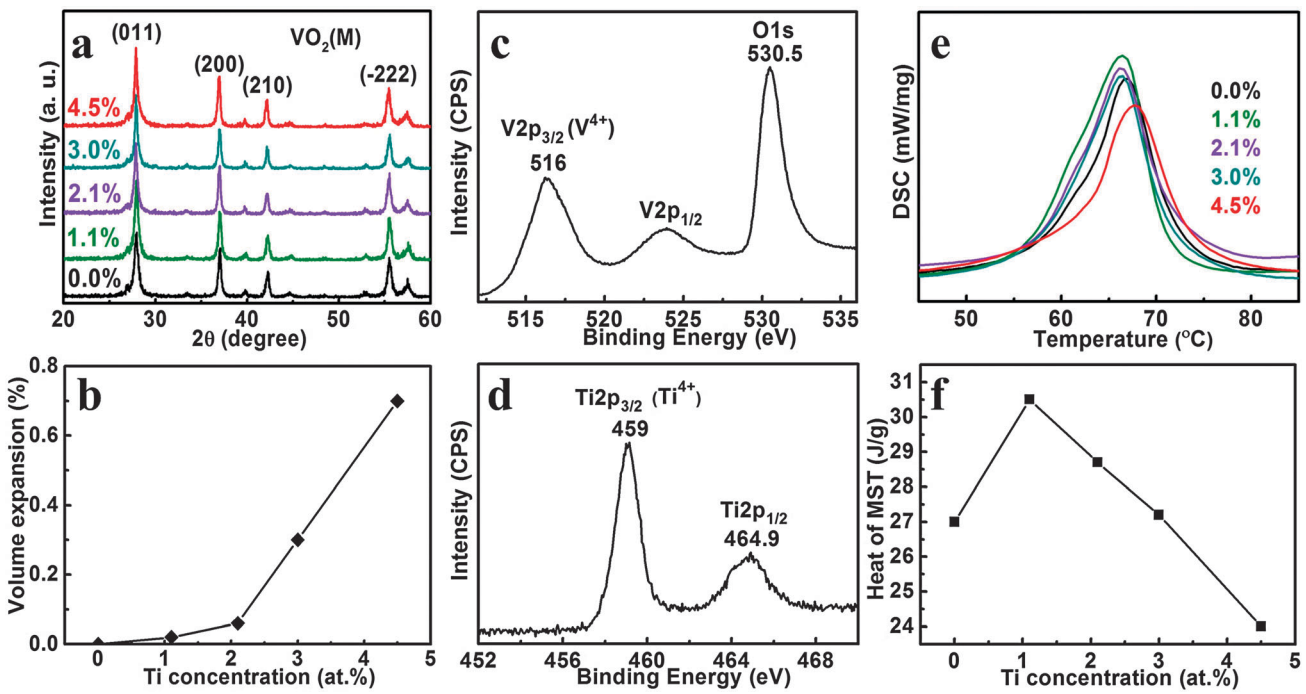

Fig. 3 The crystalline structures, XPS spectra and phase transition properties of $Ti_xV_{1-x}O_2$ samples. (a) XRD patterns. (b) Volume expansion of Ti-doped VO_2 with different concentrations. Core level spectra of V 2p (c) and Ti 2p (d) for 1.1% Ti-doped VO_2. (e) DSC curves. (f) Heat of metal–semiconductor transition (MST) of Ti-doped VO_2 with different concentrations.

 This journal is © the Owner Societies 2013

Published on 12 September 2013. Downloaded by Michigan State University on 20/01/2016 02:50:59.

Table 2 Lattice parameters experimentally obtained for $Ti_{1-x}V_xO_2$ samples

Ti content (%)	a (Å)	b (Å)	c (Å)	α (deg)	β (deg)	γ (deg)	V (Å^3)
0.0	5.742	4.528	5.344	90.0	122.4	90.0	117.31
1.1	5.745	4.523	5.354	90.0	122.5	90.0	117.33
2.1	5.746	4.519	5.366	90.0	122.6	90.0	117.38
3.0	5.752	4.515	5.368	90.0	122.4	90.0	117.71
4.5	5.768	4.510	5.371	90.0	122.3	90.0	118.10

DSC analysis (Fig. 3e) exhibited the phase transition temperature (T_c) of 66.9 °C for the undoped VO_2, which was close to previously reported values.[44,45] The T_c remained essentially unchanged with increasing Ti content, which may have been expected from the small volumetric expansion (<0.7%) and relatively unchanged electronic structure found at these doping levels. The heat of the metal–semiconductor transition (MST) (Fig. 3f) increased from 27 J g^{-1} to 30.5 J g^{-1} at 1.1% doping, but it decreased to 27.2 J g^{-1} at 3.0% doping and further to 24 J g^{-1} at 4.5% doping. The value at 4.5% doping is smaller than that measured for pure VO_2. The heat of MST reflected the capability of VO_2 nanoparticles to undergo this phase transition and, to a large extent, determined the ΔT_{sol} of the VO_2-nanoparticle-derived foil. As such, the increased values of the heat of MST below 3.0% Ti doping supported the increase in the ΔT_{sol} at the same doping levels.

Whereas the heat of MST can be used to characterize the crystallinity of pure VO_2,[46] this value in doped VO_2 depends on both the crystallinity and the doping-induced retardation of the phase transition. The crystallinity of VO_2 nanoparticles was fine according to the XRD pattern and TEM images, but the calculated heat of MST (51 J g^{-1}) indicated the possibility of improvement.[47] Ti doping below 3.0% resulted in a relatively small retardation of the phase transition, likely as a result of the low doping level and the similar ionic properties (radius and valence state) of V^{4+} and Ti^{4+}. This low-level doping promoted the formation of VO_2 (M) and enhanced the crystallinity of the material, in agreement with our previous work,[48] leading to an increase in the heat of MST. However, when Ti doping approached 4.5%, the resultant retardation of the phase transition became more important than the improvement in crystallinity, resulting in a decrease in the heat of MST known for heavily doped VO_2 systems.[23,44] This analysis may help to explain the increase in the heat of MST below 3% Ti doping.

The morphology of the Ti-doped VO_2 nanoparticles (1.1% doping) is primarily spherical with a small number of observed nanorods (Fig. 4a). The SAED analysis (the inset in Fig. 4a) confirmed the formation of single crystal VO_2 (M1), which is in agreement with the XRD pattern. The high-resolution TEM images (Fig. 4b) verified the high degree of crystallinity. EDS results (Fig. 3c) confirmed the existence of Ti with a relatively uniform distribution in the VO_2 crystalline structure (Fig. 4d).

Density Functional Theory (DFT) calculations were performed to understand the effects of Ti doping on the optical properties of Ti-doped VO_2. Two large supercells ($TiV_{95}O_{192}$ and $TiV_{31}O_{96}$) were constructed with 1 : 1 (Ti : V) ionic substitution and Ti concentrations corresponding to doping levels of 1.0%

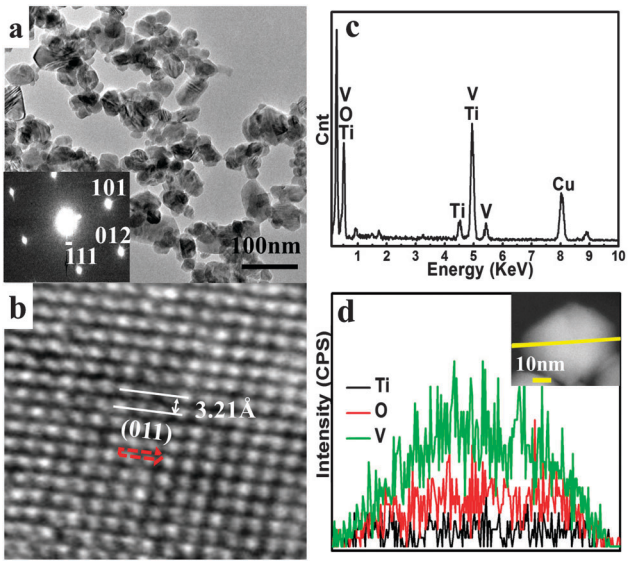

Fig. 4 TEM, HRTEM, SAED patterns and EDS results of 1.1% Ti-doped VO_2. (a) TEM (inset, SAED pattern). (b) HRTEM. (c) EDS results. (d) The compositional scanning TEM curves of a Ti-doped VO_2 nanoparticle (inset).

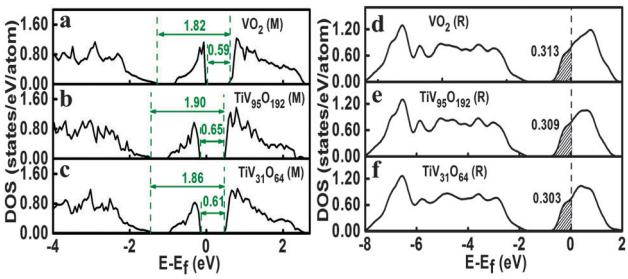

Fig. 5 Theoretical calculations. The total density of states for (a) VO_2 (M), (b) $TiV_{95}O_{192}$ (M), (c) $TiV_{31}O_{64}$ (M), (d) VO_2 (R), (e) $TiV_{95}O_{192}$ (R) and (f) $TiV_{31}O_{64}$ (R), $TiV_{95}O_{192}$ and $TiV_{31}O_{96}$ corresponding to 1.0% and 3.1% Ti. The shadow area means the electron density at Fermi level of VO_2 (R).

and 3.1%. Comparisons of the total densities of states (DOSs) of M/R-phase VO_2, $TiV_{95}O_{192}$ and $TiV_{31}O_{96}$ (Fig. 5) suggested several findings. First, as shown in Fig. 5a–c, the optical band gap (E_π, band gap between O_{2p} and π^*), corresponding to visible absorption, was 1.82 eV for VO_2 (M), in agreement with reported data.[24,49–51] However, the E_π slightly increased to 1.90 eV and 1.86 eV for $TiV_{95}O_{192}$ (M) and $TiV_{31}O_{96}$ (M), respectively. These increases implied a reduction of visible absorption (enhancement of T_{vis}) consistent with the experiment (Fig. 1c).

Second, the calculated intrinsic band gap (E_g) for pure VO_2 (M) was 0.59 eV, which was comparable to previous experimental and computational results.[52,53] Calculated E_g values of 0.65 and 0.61 eV were ascribed to $TiV_{95}O_{192}$ (M) and $TiV_{31}O_{96}$ (M), respectively. According to previous reports on the optical transmittance of VO_2 films, absorption in the near infrared region (750–1500 nm) is due to optical transitions across the intrinsic band gap.[54,55] Compared to pure VO_2, the increase in E_g for the doped materials indicates a decrease in their near infrared absorption and, as such, enhanced near infrared

Published on 12 September 2013. Downloaded by Michigan State University on 20/01/2016 02:50:59.

transmittance (T_{ni}, integral transmittance between 750 nm and 1500 nm) consistent with the increased T_{ni} at 25 °C (Fig. 1b).

Third, the electron density of VO_2 (R), $TiV_{95}O_{192}$ (R) and $TiV_{31}O_{96}$ (R) at the Fermi level (E_f) were 0.313, 0.309 and 0.303 states per atom (Fig. 5d–f), respectively, indicating that the electron density of VO_2 (R) gradually declined with increasing Ti doping. The plasma frequency of VO_2 (R) in polycrystalline thin films was reported to be 1.0 eV (~1240 nm)[56] or 1.6 eV (~775 nm),[57] considered proportional to the electron concentration in the material. With the increase of Ti doping, the decreased plasma frequency due to reduced electron density resulted in a reduction of the plasma resonance absorption between 775 nm and 1240 nm, as expected from the gradual increase of T_{ni} at 90 °C (Fig. 1b).

In summary, the increase in the optical band gap of VO_2 (M) resulted in an improvement of T_{vis}. The enhanced intrinsic band gap of VO_2 (M) led to a distinct increase of T_{ni} at 25 °C and the reduced electron density at the Fermi level of VO_2 (R) brought about a gradual improvement of T_{ni} at 90 °C. However the increase of T_{ni} at 25 °C was larger than that at 90 °C (Fig. 1b), thus the increased ΔT_{ni} resulted in the enhancement of ΔT_{sol}. Calculations well explained the change of transmittance spectra and supported the increase of T_{vis} and ΔT_{sol}.

Conclusions

Ti-doped VO_2 nanoparticles were successfully prepared *via* hydrothermal synthesis and were further used to prepare flexible solar modulation foils. EDS data and compositional scanning TEM curves confirmed the inclusion of Ti in the VO_2 lattice. The 1.1% Ti-doped foil exhibited a T_{vis} of 53% and a ΔT_{sol} of 17.2%, representing the best performance thus far reported for VO_2 foils or films prepared using available methods. The results also suggested that only a defined doping level of less than 3% was beneficial for simultaneous improvement of T_{vis} and ΔT_{sol}. The XPS results indicated that Ti^{4+} doping maintained the electronic structure stability of VO_2. The increased values of the heat of MST below 3% Ti doping support the increase in the ΔT_{sol} at the same doping levels. First principle calculations well explained the change of transmittance spectra and supported the increase of T_{vis} and ΔT_{sol}.

Acknowledgements

This study was supported in part by funds from MOST (2009CB939904, 2012AA030305, 2012BAA10B03) and NSFC (Contract No: 51172265, 51032008).

References

1 P. V. Kamat, *J. Phys. Chem. Lett.*, 2011, **2**, 839–840.
2 J. Nag and R. F. Haglund, *J. Phys.: Condens. Matter*, 2008, **20**, 264016.
3 C. Wu and Y. Xie, *Energy Environ. Sci.*, 2010, **3**, 1191–1206.
4 C. Z. Wu, J. Dai, X. D. Zhang, J. L. Yang, F. Qi, C. Gao and Y. Xie, *Angew. Chem., Int. Ed.*, 2010, **49**, 134–137.
5 C. Z. Wu and Y. Xie, *Chem. Commun.*, 2009, 5943–5957.
6 C. Wu, F. Feng and Y. Xie, *Chem. Soc. Rev.*, 2013, **42**, 5157–5183.
7 M. Kamalisarvestani, R. Saidur, S. Mekhilef and F. S. Javadi, *Renew. Sustainable Energy Rev.*, 2013, **26**, 353–364.
8 E. S. Lee, X. Pang, S. Hoffmann, H. Goudey and A. Thanachareonkit, *Sol. Energy Mater. Sol. Cells*, 2013, **116**, 14–26.
9 S. Y. Li, G. A. Niklasson and C. G. Granqvist, *Thin Solid Films*, 2012, **520**, 3823–3828.
10 L. T. Kang, Y. F. Gao, H. J. Luo, Z. Chen, J. Du and Z. T. Zhang, *Acs Appl. Mater. Interfaces*, 2011, **3**, 135–138.
11 S. Y. Li, G. A. Niklasson and C. G. Granqvist, *J. Appl. Phys.*, 2010, **108**, 063525.
12 J. Du, Y. F. Gao, H. J. Luo, Z. T. Zhang, L. T. Kang and Z. Chen, *Sol. Energy Mater. Sol. Cells*, 2011, **95**, 1604–1609.
13 Z. Chen, Y. F. Gao, L. T. Kang, J. Du, Z. T. Zhang, H. J. Luo, H. Y. Miao and G. Q. Tan, *Sol. Energy Mater. Sol. Cells*, 2011, **95**, 2677–2684.
14 N. R. Mlyuka, G. A. Niklasson and C. G. Granqvist, *Sol. Energy Mater. Sol. Cells*, 2009, **93**, 1685–1687.
15 N. R. Mlyuka, G. A. Niklasson and C. G. Granqvist, *Phys. Status Solid A*, 2009, **206**, 2155–2160.
16 N. R. Mlyuka, G. A. Niklasson and C. G. Granqvist, *Appl. Phys. Lett.*, 2009, **95**, 171909.
17 W. Burkhardt, T. Christmann, S. Franke, W. Kriegseis, D. Meister, B. K. Meyer, W. Niessner, D. Schalch and A. Scharmann, *Thin Solid Films*, 2002, **402**, 226–231.
18 M. Mao, W. X. Huang, Y. X. Zhang, J. Z. Yan, Y. Luo, Q. W. Shi and J. H. Cai, *J. Inorg. Mater.*, 2012, **27**, 891–896.
19 T. J. Hanlon, J. A. Coath and M. A. Richardson, *Thin Solid Films*, 2003, **436**, 269–272.
20 M. Nishikawa, T. Nakajima, T. Kumagai, T. Okutani and T. Tsuchiya, *Jpn. J. Appl. Phys.*, 2011, **50**, 01BE04.
21 M. Nishikawa, T. Nakajima, T. Kumagai, T. Okutani and T. Tsuchiya, *J. Ceram. Soc. Jpn.*, 2011, **119**, 577–580.
22 K. A. Khan and C. G. Granqvist, *Appl. Phys. Lett.*, 1989, **55**, 4–6.
23 J. D. Zhou, Y. F. Gao, X. L. Liu, Z. Chen, L. Dai, C. X. Cao, H. J. Luo, M. Kanahira, C. Sun and L. M. Yan, *Phys. Chem. Chem. Phys.*, 2013, **15**, 7505–7511.
24 S. L. Hu, S. Y. Li, R. Ahuja, C. G. Granqvist, K. Hermansson, G. A. Niklasson and R. H. Scheicher, *Appl. Phys. Lett.*, 2012, **101**, 201902.
25 H. Kakiuchida, P. Jin and M. Tazawa, *Thin Solid Films*, 2008, **516**, 4563–4567.
26 W. L. Hu, G. Xu, J. W. Ma, B. Xiong and J. F. Shi, *Acta Phys.-Chim. Sin.*, 2012, **28**, 1533–1538.
27 J. Du, Y. Gao, H. Luo, L. Kang, Z. Zhang, Z. Chen and C. Cao, *Sol. Energy Mater. Sol. Cells*, 2011, **95**, 469–475.
28 M. Soltani, M. Chaker, E. Haddad, R. V. Kruzelecky and J. Margot, *Appl. Phys. Lett.*, 2004, **85**, 1958–1960.
29 Y. F. Gao, S. B. Wang, H. J. Luo, L. Dai, C. X. Cao, Y. L. Liu, Z. Chen and M. Kanehira, *Energy Environ. Sci.*, 2012, **5**, 9947.
30 Y. F. Gao, S. B. Wang, L. T. Kang, Z. Chen, J. Du, X. L. Liu, H. J. Luo and M. Kanehira, *Energy Environ. Sci.*, 2012, **5**, 8234–8237.

 This journal is © the Owner Societies 2013

Published on 12 September 2013. Downloaded by Michigan State University on 20/01/2016 02:50:59.

31 G. Kresse and J. Furthmuller, *Phys. Rev. B: Condens. Matter Mater. Phys.*, 1996, **54**, 11169–11186.
32 G. Kresse and J. Furthmuller, *Comput. Mater. Sci.*, 1996, **6**, 15–50.
33 G. Kresse and D. Joubert, *Phys. Rev. B: Condens. Matter Mater. Phys.*, 1999, **59**, 1758–1775.
34 S. L. Dudarev, G. A. Botton, S. Y. Savrasov, C. J. Humphreys and A. P. Sutton, *Phys. Rev. B: Condens. Matter Mater. Phys.*, 1998, **57**, 1505–1509.
35 W. E. Pickett, S. C. Erwin and E. C. Ethridge, *Phys. Rev. B: Condens. Matter Mater. Phys.*, 1998, **58**, 1201–1209.
36 R. J. O. Mossanek and M. Abbate, *Phys. Rev. B: Condens. Matter Mater. Phys.*, 2006, **74**, 125112.
37 J. Wei, H. Ji, W. H. Guo, A. H. Nevidomskyy and D. Natelson, *Nat. Nanotechnol.*, 2012, **7**, 357–362.
38 C. A. Gueymard, *Sol. Energy*, 2001, **71**, 325–346.
39 C. A. Gueymard, D. Myers and K. Emery, *Sol. Energy*, 2002, **73**, 443–467.
40 G. Xu, P. Jin, M. Tazawa and K. Yoshimura, *Appl. Surf. Sci.*, 2005, **244**, 449–452.
41 L. T. Kang, Y. F. Gao and H. J. Luo, *ACS Appl. Mater. Interfaces*, 2009, **1**, 2211–2218.
42 G. Silversmit, D. Depla, H. Poelman, G. B. Marin and R. De Gryse, *J. Electron Spectrosc. Relat. Phenom.*, 2004, **135**, 167–175.
43 P. S. Liu, W. P. Cai, L. X. Wan, M. D. Shi, X. D. Luo and W. P. Jing, *Trans. Nonferrous Met. Soc. China*, 2009, **19**, S743–S747.
44 L. Chen, C. Huang, G. Xu, L. Miao, J. Shi, J. Zhou and X. Xiao, *J. Nanomater*, 2012, **2012**, 491051, DOI: 10.1155/2012/491051.
45 H. Miyazaki, K. Yoshida, S. Sasaki, N. Sakamoto, N. Wakiya, H. Suzuki and T. Ota, *J. Ceram. Soc. Jpn.*, 2011, **119**, 522–524.
46 Y. Kong and J. N. Hay, *Polymer*, 2002, **43**, 3873–3878.
47 J. Cao, Y. Gu, W. Fan, L. Q. Chen, D. F. Ogletree, K. Chen, N. Tamura, M. Kunz, C. Barrett, J. Seidel and J. Wu, *Nano Lett.*, 2010, **10**, 2667–2673.
48 Y. F. Gao, C. X. Cao, L. Dai, H. J. Luo, M. Kanehira, Y. Ding and Z. L. Wang, *Energy Environ. Sci.*, 2012, **5**, 8708–8715.
49 Z. Luo, Z. Wu, X. Xu, T. Wang and Y. Jiang, *J. Vac. Sci. Technol., A*, 2010, **28**, 595–599.
50 H. Abe, M. Terauchi, M. Tanaka, S. Shin and Y. Ueda, *Jpn. J. Appl. Phys.*, 1997, **36**, 165–169.
51 W. Z.-M. Luo Zhen-Fei, X. Xiang-Dong, W. Tao and J. Ya-Dong, *Chin. Phys. B*, 2010, **19**, 106103.
52 T. C. Koethe, Z. Hu, M. W. Haverkort, C. Schussler-Langeheine, F. Venturini, N. B. Brookes, O. Tjernberg, W. Reichelt, H. H. Hsieh, H. J. Lin, C. T. Chen and L. H. Tjeng, *Phys. Rev. Lett.*, 2006, **97**, 116402.
53 S. Biermann, A. Poteryaev, A. I. Lichtenstein and A. Georges, *Phys. Rev. Lett.*, 2005, **94**, 026404.
54 M. M. Qazilbash, A. A. Schafgans, K. S. Burch, S. J. Yun, B. G. Chae, B. J. Kim, H. T. Kim and D. N. Basov, *Phys. Rev. B: Condens. Matter Mater. Phys.*, 2008, **77**, 115121.
55 K. Okazaki, S. Sugai, Y. Muraoka and Z. Hiroi, *Phys. Rev. B: Condens. Matter Mater. Phys.*, 2006, **73**, 165116.
56 M. Kang, S. W. Kim, J. W. Ryu and T. Noh, *AIP Adv.*, 2012, **2**, 012168.
57 B. Felde, W. Niessner, D. Schalch, A. Scharmann and M. Werling, *Thin Solid Films*, 1997, **305**, 61–65.